Adiabatic Energy Loss in Hyperthermal H Atom Collisions with Cu and Au: a Basis for Testing the Importance of Nonadiabatic Energy Loss

Michele Pavanello[1,†], Daniel J. Auerbach[1,2,3,], Alec M. Wodtke[2,3], Maria Blanco-Rey[4,5], Maite Alducin[5,6], and Geert-Jan Kroes[1]*

[1]Leiden Institute of Chemistry, Gorlaeus Laboratories, Leiden University, P.O. Box 9502, 2300 RA Leiden, The Netherlands

[2]Max Planck Institute for Biophysical Chemistry, Göttingen, Germany

[3]Institute for Physical Chemistry, Georg-August University of Göttingen, Göttingen, Germany

[4]Departamento de Física de Materiales, Facultad de Químicas UPV/EHU, Apartado 1072, 20018 Donostia-San Sebastián, Spain

[5]Donostia International Physics Center, Paseo Manuel de Lardizabal 4, 20018 Donostia-San Sebastián, Spain

[6]Centro de Física de Materiales, Centro Mixto CSIC-UPV/EHU, Paseo Manuel de Lardizabal 5, 20018 Donostia-San Sebastián, Spain

Definitions concerning the scattering of H from the (111) surface of Cu and Au.

All calculations discussed in this work are performed for H scattering from the (111) face of either Cu or Au. The incidence angle θ_i and the scattering angles θ_f and ϕ_f are shown in Fig.S1A, and the structure of the (111) surface is shown in Fig.S1B. Fig.S1B also shows the high symmetry sites top (first layer atom), hcp (the hollow site above a second layer atom), fcc (the hollow site above a third layer atom), and bridge (brg, a site midway between two neighbouring top sites). The (111) surface of an fcc metal has the well-known stacking ...ABCA... so that atoms in the fourth layer are beneath atoms in the first layer.

The "t2h" and "t2f" sites are midway between neighbouring top and hcp sites and midway between neighbouring top and fcc sites, respectively.

In our calculations we use two coordinate systems, i.e., a lab frame and a reference frame. In the right handed coordinate system describing the lab frame, the Z-axis points perpendicularly away from the surface, and the X-axis is in the $[10\bar{1}]$ crystallographic direction, pointing in the direction shown in Fig.S1B. The polar angle of incidence, θ_i, and the polar scattering angle, θ_f, can both be defined relative to this coordinate system, as indicated in Fig.S1A. As also indicated in Fig.S1A, we follow an often used convention in surface science in which both polar angles are taken in the range [0°,90°]. Both angles are defined relative to the surface normal (the Z-axis), for instance, $\theta_i = 0°$ means H is incident normal to the surface.

The azimuthal incidence angle ϕ_i defines the orientation of the incidence plane relative to the lab frame. Specifically, the reference frame is the right handed coordinate system X'Y'Z in which the incidence of H is along the X'Z plane, in the positive X' direction. Furthermore, the X' and Y' axes can be obtained by rotating the X and Y axis around the Z-axis in counter-clockwise fashion over ϕ_i. This incidence angle is therefore referenced to the $[10\bar{1}]$ direction, i.e., incidence along this direction means $\phi_i = 0°$. For $\phi_i = 30°$, incidence is in the $[11\bar{2}]$ direction (see Fig.S1B). A crucial point is that for $\phi_i = (30 \pm 120\ n)°$, n being an integer, an H-atom flying over the surface along the line passing neighbouring top, hcp, bridge, and fcc sites samples these sites in the order top, hcp, bridge, and fcc. In contrast, $\phi_i = (90 \pm 120\ n)°$ describes the situation in which the H-atom flying along such a line samples the sites in the order top, fcc, bridge, and hcp.

The azimuthal scattering angle ϕ_f (See Fig. 1A) is referenced to the particular incidence direction considered, which depends on the value of ϕ_i and ϕ_f takes values between -180° and 180°. With this convention, $\phi_f = 0°$ corresponds to forward in-plane scattering, and specular scattering occurs for $\phi_f = 0°$ and $\theta_f = \theta_i$. In contrast, $\phi_f = 180°$ corresponds to backward in-plane scattering and $\phi_f = 90°$ to side-ways scattering (as already noted θ_f and θ_i are taken to lie in the range [0°,90°]). Note that with the convention adopted, for incidence with $\phi_i = (30 \pm 60\ n)°$ the scattering distributions for the final scattering angles $+\phi_f$ and $-\phi_f$ are equal by symmetry, while they are expected to differ for $\phi_i = (0 \pm 60\ n)°$. With the conventions adopted, the Cartesian components of the initial and final velocities $\vec{v}_i$ and $\vec{v}_f$ may be written in the lab frame as

$$v_{ix} = v_i \sin\theta_i \cos\phi_i$$
$$v_{iy} = v_i \sin\theta_i \sin\phi_i$$
$$v_{iz} = -v_i \cos\theta_i,$$

and

$$v_{fx} = v_f \sin\theta_f \cos(\phi_i + \phi_f)$$
$$v_{fy} = v_f \sin\theta_f \sin(\phi_i + \phi_f)$$
$$v_{fz} = v_f \cos\theta_f,$$

where v_i and v_f are the magnitudes of the initial and final velocity, respectively. Note that the minus sign in front of the negative z-component of the initial velocity is simply a consequence of the often used convention in surface science that θ_i be in the range [0°,90°]

even though strictly speaking the incident velocity vector makes an angle of (180° - θ_i) with the surface normal.

Electronic structure calculations.

To obtain energies and forces, electronic structure calculations were performed using a modified version of the VASP code [1-4], which makes use of density functional theory (DFT) [5-6]. To describe the exchange-correlation energy of the electrons we have used the generalized gradient approximation (GGA). In applying the GGA we have used a mixture of two of the most popular functionals in molecule/surface interaction studies, the PBE [7] and the RPBE functional [8], with exchange correlation-functionals E_{XC}^{PBE} and E_{XC}^{RPBE}, as follows

$$E_{XC}^{SRP} = xE_{XC}^{RPBE} + (1-x)E_{XC}^{PBE} \qquad (1).$$

The functional used here (which we call SRP48, with $x = 0.48$) has been designed to accurately describe the reactive interaction of H_2 with Cu(111) [9-10] and has been shown to be transferable to the H_2 + Cu(100) system [11]. For the sake of consistency we therefore also use this functional for H + Cu(111), and because Au is a noble metal like Cu we also use it for H + Au(111). Here, the hope is that the SRP48 functional describes the interaction between the s-orbitals of H and the d-orbitals of Cu as accurately as it does the interaction of the $1\sigma_g$ and $1\sigma_u$ orbitals of H_2 with the d-orbitals of Cu.

In the DFT calculations, the ion cores were described using nonlocal ultrasoft pseudopotentials [12] computed with the PW91 functional and taken from the database

supplied with the VASP code. Using a pseudo-potential computed with one GGA (PW91) in calculations employing a different GGA (the SRP48 functional[10], see Eq.1) is expected to lead to errors in the molecule-surface interaction energy that are less than 30 meV, and probably smaller than that. We base this on calculations performed by Hammer et al. on O/Pd(111) and CO/Pd(111)[8] that found errors smaller than 30 meV if LDA pseudo-potentials were used in calculations with the PW91 functional instead of PW91 pseudo-potentials. We also base this on the assumption that errors will be smaller if a pseudo-potential computed with a different GGA functional is used in a GGA calculation than if a LDA-pseudopotential is used in a GGA calculation, especially if the GGAs used in the pseudo-potential and in the overall calculation are rather similar, as is the case here. The electronic orbitals were described by a plane wave basis set. To model the adsorbate/substrate system a four-layer metal (Cu or Au) slab was used together with a (2x2) surface unit cell.

A geometry optimization of bulk copper using the SRP48 functional yields a bulk lattice constant of 3.68 Å, the experimental value being 3.61 Å for Cu. For bulk Au the computed lattice constant was 4.20 Å, compared with an experimental value of 4.08 Å [13]. Thus, the 0K surface lattice constant used was $3.68/\sqrt{2}$ = 2.60 Å for Cu (2.97 Å for Au), and the computed bulk interlayer distance is $3.68/\sqrt{3}$ = 2.1244 Å for Cu (2.43 Å for Au). For Cu, interlayer distances of the slab were allowed to relax to values of d_{12} = 2.1009, d_{23} = 2.1038, and d_{34} = 2.1012 Å for the distances between layers 1 and 2, 2 and 3, and 3 and 4, respectively. The computed contraction of the distance between layers 1 and 2 of the Cu(111) surface (1.1%) is in good agreement with medium-energy ion-scattering results obtained for room temperature [14]. For Au, interlayer distances of the slab were allowed to relax to values of d_{12} = 2.4465, d_{23} =2.4014, and d_{34} = 2.4474. The percentage difference of

d_{12} with the computed bulk interlayer distance is less than 1%. This is in line with previous calculations [15-16] and XRD experiments [17], with less accurate LEED experiments not showing a deviation [18].

First, we carried out static (single-point) DFT calculations on H + Cu(111) and Au(111). In these calculations, the metal atoms were kept frozen at their positions in the relaxed bare metal slab, but the position of the H-atom was varied. A vacuum layer of 13.0 Å was placed between the slabs in the Z direction to avoid artifacts caused by the use of periodic boundary conditions in the direction perpendicular to the slab. An 8x8x1 grid of shifted (Γ-centered) Monkhorst-Pack *k*-points [19] was used to sample the Brillouin zone and a cut-off energy of 350 eV for the plane-wave expansion. For fast convergence of the calculations, a Fermi level smearing of 0.1 eV was used. The convergence of the calculations is similar to that discussed in Ref.[9], i.e., we estimate that our H-atom surface interaction energies are converged to within approximately 60 meV with respect to the input parameters discussed above (thickness of slab, size of surface unit cell, numbers of k-points, etc.).

Calculations on H + Cu(111) and Au(111) differ from calculations on H_2 + Cu(111) in that far away from the surface (for Cu this is for $Z \geq 2.25$ Å, Z being the atom surface distance), H may retain (part of) its electron spin, so that spin polarized calculations are required. For Cu and for $Z < 2.25$ Å, spin unpolarized calculations (S=0) and spin polarized calculations yield electronic energies that are identical to within the convergence limit imposed in the calculations. For Au, spin polarized and spin unpolarized calculations yield identical energies for $Z \leq 2.0$ Å. A problem we found for both Cu and Au is that in the range $2.0 \text{ Å} \leq Z \leq 3.0$ Å the H + Me(111) interaction energy may not converge well with the default settings used in the charge density mixing [4], in the iterative solution of the

Kohn-Sham equations. This problem may be resolved by effectively using linear mixing of the old and new densities in obtaining the new density in the iterations. This is done by taking the VASP input parameters AMIX and BMIX as 0.3 and 0.0001, respectively, and by taking the input parameters AMIXMAG and BMIXMAG also as 0.3 and 0.0001, respectively, in the use of the Pulay mixer [20], which employs an initial approximation for the charge dielectric function according to Kerker [21]. See also Ref.[22].

Using single point calculations with the surface taken as static and as described above, potential curves were mapped out for H being above or below the top, bridge, fcc hollow, hcp hollow, and t2f and t2h sites (where, as stated earlier, the latter two are midway between top and fcc sites, and top and hcp sites, respectively, see also Fig.S1). These potential curves are shown in Figs. S2 and S3, for H + Cu(111) and Au(111), respectively. For both Cu and Au the potential minima were obtained for H being above the fcc site and above the surface, the minimum interaction energy being - 2.37 eV for Cu(111) and -1.97 eV for Au(111), respectively. These values are in reasonable agreement with recent DFT calculations employing the PW91 functional that yield energy minima of -2.45 eV and -2.18 eV [23], if one takes into account that the PW91 functional tends to overestimate adsorption energies. This should be corrected for at least in part in the present work by mixing in the more repulsive RPBE functional [8]. The minimum interaction energy for H + Cu(111) (-2.37 eV) is also in good agreement with estimates of the well depth that are based on experiments. According to the analysis of experiments by Hammer and co. [24], the well depth should fall in the range 2.4-2.5 eV. The only value we have for the experimental H + Au(111) well depth (2.39 eV) comes from temperature programmed desorption (TPD) experiments [25]. This value was derived using the Redhead approximation [26], a desorption temperature of 210 K, and an assumed frequency factor of 10^{13} s^{-1}. It is not clear to us how

reliable this value is, as peaks in TPD spectra for associative desorption cannot always be straightforwardly interpreted in terms of the binding energy of the individual atoms to the surface [27]. Assuming the experimental value (or rather its range) for H + Cu(111) and the PW91 energy differences reported by Mavrikakis and co. [23] to be reliable, the value of the well depth for H + Au(111) should be in the range 2.03-2.13 eV, which is in much better agreement with the value we find for H + Au(111) (1.97 eV).

We also performed a Bader charge analysis [28] for H above and in Au(111) along the same lines of approach as used in the single-point calculations discussed above. This analysis showed close to zero charges on the H-atom for all investigated geometries. The observation of close to zero Bader charges means that it is unnecessary to supplement the interaction potential (forces) computed with DFT in the AIMD calculations with image-charge interaction correction terms, as often done in simulations of high-energy scattering of ions from metal surfaces [29]. The observation of close to zero charge on H interacting with Au can be explained from H and Au exhibiting a similar electronegativity. For the same reason, hydrogen forms polymeric covalent hydrides with Au and Cu [30].

Ab Initio Molecular Dynamics (AIMD) method.

In the AIMD method used here, dynamical quantities are computed using classical dynamics for nuclear motion while computing the forces on the fly using DFT. AIMD calculations were first used to model a surface reaction by De Vita et al. [31], who computed 5 trajectories to model dissociative chemisorption of Cl_2 on Si(111). Statistically meaningful results, i.e., reaction probabilities with reasonably small statistical errors, were first obtained for a reaction of a molecule on a metal surface by Groß and Dianat in 2007

[32]. In the latter calculation and in most subsequent AIMD calculations aimed at calculating reactive scattering probabilities [33-36], on which the discussion below is focused, the surface atoms were taken initially at rest (T_s = 0 K), and spin unpolarized DFT calculations were done. Only in 2012 were AIMD calculations performed for a molecule impinging on a hot surface [10]. Likewise, only in 2012 Groß reported preliminary AIMD calculations in which spin polarized DFT was used to model O_2 dissociation over a Pt surface [37]. The calculations here performed include both of these non-standard features, i.e., they were performed for a non-zero initial surface temperature, and used spin polarized DFT. These features complicate the calculations. As detailed below, an algorithm needs to be used to sample the displacements and momenta of the surface atoms according to the pre-defined temperature. Furthermore, as noted by Groß spin polarized DFT calculations require twice as many basis functions to model both the spin-up and spin-down components, and typically it is harder to converge the self-consistent field iteration to solve the Kohn-Sham equations [37]. Below, we discuss an additional complication with spin polarized calculations, which arises if a rebounding H-atom recovers its spin.

In the AIMD calculations, the Cu (Au) substrate was modeled using 4 layers as in the static surface calculations discussed above, and more generally all input parameters to the electronic structure part of VASP were taken the same as discussed above. Of the 4 layers, only the upper 3 layers were allowed to move. Molecular dynamics simulations were performed using the Verlet algorithm [38-39] with a time-step of 1.0 fs in the equilibration of the copper and gold surfaces discussed below.

Experiments [40-41] show that, going from 0 K to the surface temperature used in the H-surface scattering simulations (T_s=120 K), a small expansion of bulk Cu occurs, the bulk

lattice constant increasing by 0.06%. In our AIMD calculations to set up surfaces for T_S=120 K, the 0K SRP48 DFT bulk lattice constant was therefore multiplied with 1.0006, to obtain the bulk lattice constant (3.6818 Å) defining the X- and Y-dimensions of the Cu-slabs for this temperature. Bulk Au expands by 0.089% going from T_S=0 to 120 K [42-44], and taking this into account in the same way as done for Cu gave a bulk lattice constant of 4.205 Å for use in the AIMD simulations.

We performed AIMD simulations of ten different Cu(111) (Au(111)) slabs, imposing a temperature on these slabs. The procedure used was as follows. The slabs were initialised by selecting displacements and velocities of the moving metal atoms from a classical Boltzmann distribution of atomic harmonic oscillators for a temperature of 120 K, according to frequencies computed from a normal mode calculation with VASP in which a single metal atom was allowed to move in the X, Y, and Z-directions in either layer 1, 2, or 3. These calculations gave frequencies in the range 16.0 – 20.5 meV for Cu(111), and in the range 8.0 to 11.0 meV for Au(111). Next, a first AIMD simulation was performed in the microcanonical ensemble (NVE, meaning that the number of particles N, the volume V, and the total energy E were all kept constant) for 1.8 ps. For both Cu and Au this resulted in an average surface temperature that was close to the one aimed at. For subsequent sampling of the metal atom coordinates and velocities, we therefore performed only one subsequent, second AIMD NVE run, for 1 ps, in which we also computed the surface temperature and the average interlayer spacing between layers 1 and 2. The surface temperatures obtained were 112.6 K for Cu(111), with a standard deviation σ of 19 K, and 133 K for Au(111), with σ = 28 K. The averages are in good agreement with the temperature we intended to impose, and the standard deviation is close to what would be expected for an ensemble containing N=36 degrees of freedom ($\sigma_T = T/\sqrt{N_d}$ = 20 K, N_d

being equal to the number of degrees of freedom of the metal atoms). The average value of d_{12} we computed for Cu was 2.110 ± 0.003 Å. This value is somewhat smaller than the SRP48 bulk interlayer distance we compute for 120 K (2.1257 Å), in good agreement with the interlayer contraction observed experimentally for room temperature (1% [14], vs. 0.7% obtained by us). For Au, the average d_{12} we computed was 2.464 ± 0.007 Å. This value is in satisfactory agreement with, but somewhat overestimates the computed bulk interlayer distance at this temperature of 2.428 Å.

For H + Cu(111) and Au(111), in our AIMD calculations we effectively used the classical trajectory (CT) method [45] to simulate the scattering of H-atoms from the surface considered, i.e., classical molecular dynamics with Monte-Carlo sampling of the appropriate initial conditions (but of course computing the forces on the fly from DFT). Scattering probabilities, for each initial incidence energy, are calculated as an average over the initial conditions (position of the atom over the surface unit cell), which are sampled using a conventional Monte Carlo procedure. We also sample over the metal surfaces we simulated, choosing 1 of 1000 configurations recorded for each surface, and one out of 10 surfaces, at random. This procedure allows us to model the effect of local variations of temperature without having to perform prohibitively expensive simulations involving too large surface unit cells. In order to obtain reasonably low statistical errors at acceptable computational cost we compute 900 trajectories per combination of incidence angle and collision energy.

The procedure used is then as follows. The H-atom is started at 6.0 Å above the surface. The maximum propagation time used is 120 fs, and the timestep 0.1 fs. We consider that scattering has taken place (i) whenever the atom bounces back to the gas phase and reaches

a distance from the surface greater than 6.1 Å (in which case the trajectory is stopped), or if (ii) after 120 fs the H-atom is moving away from the surface at $Z \geq 3.3$ Å, and its normal kinetic energy exceeds the H-Me(111) interaction computed for a static surface and averaged over the top, bridge, fcc, hcp, t2f, and t2h sites by 50 meV at the current value of Z. Trajectories in which the H-atoms fly through the 4-layer slab are classified as "fly through". The outcome of trajectories that fall in neither of these two categories is classified as "unclear", these trajectories might still result in scattering or flying through the slab, or the outcome may be that H remains in or on the slab (absorption or adsorption). An important point about the unclear trajectories is that even if the H-atom has not yet entered the surface after 120 fs it may still do so later, so that the outcome can be scattered without or with penetration. In contrast, if the H-atom has entered the surface by that time, an unclear trajectory may still lead to scattering with penetration, but not to scattering without penetration of the surface.

The scattered trajectories may be further subdivided as follows. We distinguish between outcomes in which the H-atoms scatter from the surface without entering the subsurface, and outcomes in which scattering occurs in a trajectory in which H enters the surface and subsequently re-emerges at the gas phase side, and leaves the surface ("scattering without penetration" and "scattering with penetration"). Here, the surface is dynamically defined, i.e., to make the distinction we compare the instantaneous Z-value of the H-atom to the instantaneous average of the four Z-values of the surface metal atoms to decide whether H goes subsurface at any point during the trajectory. We may also distinguish between direct and indirect scattering trajectories. In a direct (indirect) trajectory, the Z-value of the H-atom exhibits one (multiple) inner turning point(s).

A complication with the AIMD calculations on H + Cu(111) and Au(111) that we observed initially was that, in our spin polarized DFT calculations, H did not regain its spin upon coming back from the surface (the magnetization remained zero). This is in accordance with the observation that plane wave DFT calculations with VASP on magnetic systems may not converge if the initial magnetization (which was zero close to the surface) is smaller than the magnetization that should result from the calculation. To solve this problem, we used a script to stop and restart the VASP AIMD calculations once the back-scattering H-atom reaches a distance from the surface > 2.05 Å for Cu, and > 1.80 Å for Au. The AIMD calculations were subsequently performed with spin polarization and starting from a trial wave function in which each atom is in its α spin state (has one unpaired electron with spin up), performing one time-step at a time until the system again had a total magnetization of 0.6 μ_B. Subsequently, the AIMD spin polarized calculations could again be performed in multistep fashion, where at each time-step a guess of the initial wave function is obtained from the converged wave function at the previous timestep, as implemented in VASP. Recognizing that computation time can be saved when the H-atom is closer to the surface, the script we developed also stops and restarts the VASP AIMD calculations whenever the H-atom gets closer to the surface than 2.05 Å for Cu, or 1.80 Å for Au. In this case, the AIMD calculations are performed in multi-step fashion using spin unpolarized DFT. At the start, the H-atom is propagated towards the surface using multi-step AIMD with spin polarized DFT.

In a minority of trajectories, we observed problems with energy conservation. We use an option in VASP that keeps the number of electronic iterations down by predicting the electronic wave function for the next time-step from the wave function at previous steps. In spin polarized calculations, the algorithm used may break down for the problem we study

if the magnetization changes rapidly with time. This may result in rapid oscillations of the magnetization, which then takes on positive and negative values, and in all cases where a problem with energy conservation occurred, the problem could be attributed to this cause. In all cases the problem was solved by restarting the AIMD simulation at a point in time where the breakdown of energy conservation had not yet occurred. Next we propagated the equations of motion in one-step mode through the critical region, after which normal time propagation was resumed. Such a restart was made if the magnetization was found to take on negative values < -0.33, or if the total energy drift exceeded 150 meV, or if the energy drift per fs exceeded 0.85 meV/fs. With the timestep and the criterion for convergence of the total energy that we used, average values of the energy drift and energy drift per fs per trajectory were 12 meV, and 0.12 meV/fs, respectively (as computed for H + Au(111) at an incidence energy of 5 eV, $\theta_i = 60°$, and incidence along the [10-1] direction).

In our calculations, artifacts could arise from the heat wave generated by the collision being reflected from the walls of the periodic surface unit cell or the static metal layer at the bottom (as noted above, the metal atoms in the bottom surface layer are kept fixed). With the width of the 2 x 2 surface unit cell used for Cu (5.20 Å) and Au (5.95 Å), and taking into account the velocity of sound in these metals (39 Å/ps for copper, 32 Å/ps for gold), this complication is avoided using the selected value of t_{max} of 120 fs. We refrain from the use of a thermal bath at the bottom of the slab (as can be done with for instance the generalized Langevin formalism [46]) as it is not clear how this would affect the collision dynamics.

Estimating the long-time contribution of H-atoms that have penetrated the surface.

In our simulations, we only count as scattered those H-atoms that within 120 fs either escape from the surface to a distance of greater than 6.1 Å, or reach at least 3.3 Å from the surface with an outward normal translational energy exceeding the estimated atom-surface interaction energy by 50 meV. However, as Table 1 shows, for H+Au(θ_i =60°, ϕ_i =0°) a substantial amount of H-atoms have entered the slab but are classified as "unclear" because they have not scattered yet (14.2%). Furthermore, a smaller amount of H-atoms have flown through our 4-layer slab (7.3%), and these should also really be counted as having penetrated the slab. Together, these catagories make up 21.5% of the incident H-atoms that might have emerged as scattered with penetration in a simulation that would have modeled more metal layers and would have been performed on a much longer timescale than was possible here.

To arrive at an estimate of how these catagories of atoms might contribute to the angularly resolved energy loss spectrum for θ_f= 60° and ϕ_f = 90° (Fig.4), energy losses of atoms scattering to this final solid angle have been computed using the following simplifying assumptions: (i) It was assumed that the remaining H-atoms would scatter to the solid angle considered in proportion to the binning range in the solid angle, $\Delta\phi_f$ being 60° and $\Delta\theta_f$ being 15°. As a result of this, probabilities that H scatters with a specific energy loss have to be divided by aan angular dilution factor $2\pi/[\pi/3\times\{\cos(\theta_f-7.5°)-\cos(\theta_f+7.5°)\}]$, which is 26.5 for θ_f= 60°. (ii) The energy lost by the H-atoms that had penetrated the surface but were classified as unclear was calculated as $\Delta E = 3\times N_{move}\times(kT_s^f - 120)$. Here N_{move} is the number of moving metal atoms, T_s^f is the surface temperature in K at the end of the trajectory, and we have

assumed equipartioning between translational and potential energy of the metal atoms. (iii) The energy lost by the H-atoms that had flown through the slab was calculated as $\Delta E = 2 \times 3 \times N_{move} \times (kT_s^f - 120)$. Here, the extra factor 2 comes from making the assumption that if the H-atom were to back up and emerge at the gas phase side it would lose the same amount of energy as on its way in.

With the assumptions made above, we probably overestimate the number of H-atoms that scatter to the specific final solid angle addressed (θ_f= 60° and ϕ_f = 90°) at long times. Our statistical approach to the angular distribution of these atoms suggests that 7 out of 194 atoms considered scatter to this final solid angle. However, none of the 126 atoms that scattered with penetration within the timescale of the simulation was found at this final solid angle. Furthermore, we probably underestimate the energy lost to the surface of the atoms expected to emerge from the surface at long times after moving into the surface. For instance, 84% of the atoms classified as unclear and having penetrated the surface remained in the gold slab at the time the trajectory was stopped, and most of these atoms would probably lose more energy to the surface before emerging from it at the gas phase side. Furthermore, the atoms that have flown through the slab in our calculation have not yet experienced the hard collision with a lower layer atom which could send the H-atom on its way back to the gas phase. The results of this conservative analysis are shown in Fig.S5.

Comparison of Fig.S5 to Fig.4 shows how the angularly resolved energy loss distribution of atoms that scatter with penetration changes if the contribution at long times is taken into account on the basis of the assumptions outlined above. Even though the figure probably overestimates the H-atoms scattering at long times to the final solid angle considered and probably underestimates their energy loss, our calculations predict that it should be

possible to measure a very well resolved low energy peak in the energy loss distribution, that can be attributed almost exclusively to H-atoms scattering without penetration. Specifically, we predict that the number of H-atoms scattering without penetration of the surface and experiencing energy losses ≤ 0.2 eV should exceed the number of H-atoms scattering with penetration of the surface and experiencing such low energy losses by about a factor 100, under the assumptions made above. This number, which most likely is an underestimate, is considerably larger than the corresponding number (30) for the energy distribution integrated over final scattering angles. The low energy peak in Fig.S5 is also much easier to measure than its counterpart in Fig.1A as it requires an experiment where the detector is placed at one final solid angle only.

We have also considered how other results for H+Au(θ_i =60°, ϕ_i =0°) change if long time contributions are taken into account from penetrated unclear trajectories and from trajectories in which the H-atoms flew through the slab. The conclusion that the adiabatic energy loss spectrum (Fig.1A) shows a fairly well resolved peak below 0.2 eV remains unchanged. However, the number of H-atoms scattering without penetration of the surface and experiencing energy losses ≤ 0.2 eV should exceed the number of H-atoms scattering with penetration of the surface and experiencing such low energy losses by only about a factor 30 if the long time contribution is taken into account, compared to a factor of about 45 without this contribution. Angular distributions like Fig.2A and Fig.3 can be corrected for the estimated long time contribution by adding the ratio of P_{pen}^{long} (0.215) divided by the angular dilution factor to the probabilities of scattering with penetration and the total scattering probabilities. This amounts to adding probabilities which vary from 0.0012 for θ_f= 7.5° to 0.0093 for θ_f= 82.5°. Once done, the probability of scattering with penetration still shows a minimum at θ_f= 60° in Fig.3, but it is no longer zero, being 0.0081.

Ab Initio Molecular Dynamics with electronic friction (AIMDEFp).

We have also used our AIMD calculations to estimate the non-adiabatic energy loss to electron-hole pair excitation, E_{NA}, in terms of a friction force. For each trajectory, the value of E_{NA} for a particular H-atom surface collision was computed after the trajectory was completed with ordinary AIMD, i.e., the friction force was applied "post" the trajectory. This is why we call these calculations "AIMDEFp". Obviously, the best approach would have been to apply the friction force on the H-atom while it is moving, i.e., in an ab initio molecular dynamics with electronic friction (AIMDEF) calculation, as suggested in [47]. However, such an approach has, to our knowledge, not yet been implemented. Instead, here we used the time-dependent H-atom coordinates $\vec{r}(t)$ and velocities $\vec{v}(t)$ from the AIMD trajectories to compute the friction force within the local density friction approximation (LDFA) [48]. Using the position-dependent friction coefficient, $\eta(\vec{r})$, the energy loss to electron-hole pair excitations incurred during the time t_c that the H-atom interacts with the surface can be computed as

$$E_{NA} = \int_{t=0}^{t} \eta(\vec{r}(t))v(t)^2 dt \qquad (2).$$

The friction coefficients used in the LDFA, which are calculated for the electronic density of the bare metal slab at $\vec{r}(t)$, have been successfully applied to understand different properties of the energy loss of atoms and ions on surfaces [49-52]. Here, an additional approximation made was that the electronic density was calculated fixing the metal atoms at their thermal equilibrium positions at T_s = 120 K.

In Fig. S6 the total energy loss distributions (integrated over all scattering angles) are shown as computed with AIMDEFp, and in Table S1 the adiabatic and non-adiabatic energy losses computed with AIMD and AIMDEFp are shown for the example we focus on, i.e. scattering of H from Au(111) at θ_i =60°, and ϕ_i =0°. A comparison to the adiabatic results shown in Fig.1 reveals dramatic differences. For instance, because in scattering of H from Au(111) at θ_i =60°, and ϕ_i =0° the energy lost to electron-hole pair excitation is almost an order of magnitude larger than the energy loss to phonons, the total energy loss spectrum in the top panel of Fig.S6 takes on a qualitatively different form from the figure describing the corresponding adiabatic case, Fig.1A. In the AIMDEFp results, the lowest energy peak now occurs near 0.4 eV instead of near 0.1 eV as observed in the adiabatic case. Also, the lowest energy peak no longer dominates the energy loss spectrum computed with AIMDEFp as it does the AIMD energy loss spectrum: the AIMDEFp spectrum shows a peak near 0.7 eV that is higher than the lowest energy peak.

Finally, it is illustrative to consider how the AIMDFp conclusions might be affected by using alternative friction coefficients. In Fig. S7 the friction coefficients we computed for the H-atom approaching Cu(111) above a first-layer surface atom are compared with the friction coefficient computed by Trail *et al.* [53] for the same system and approach symmetry, but using a different theoretical approach. The agreement between both methods is reasonable at small atom surface distance values, but at larger distances their friction coefficient is larger than ours because of the peak appearing in their calculation at Z=2.5Å. To obtain the friction coefficient at these distances, Trail *et al.* had to fix the spin of the approaching H-atom to its gas phase value, in order to avoid a singularity in the friction coefficient that otherwise arises in their theory due to the spin transition that DFT predicts at values around z=2.5A.

Regardless of this, it is likely that with their method an even greater average energy loss would be obtained for H-atoms that scatter without penetration in the surface than with our method. Therefore, the main conclusion we draw, i.e., that including electron-hole pair excitation in the theoretical description leads to far greater energy loss of H-atoms that scatter without penetration of the surface, is not altered.

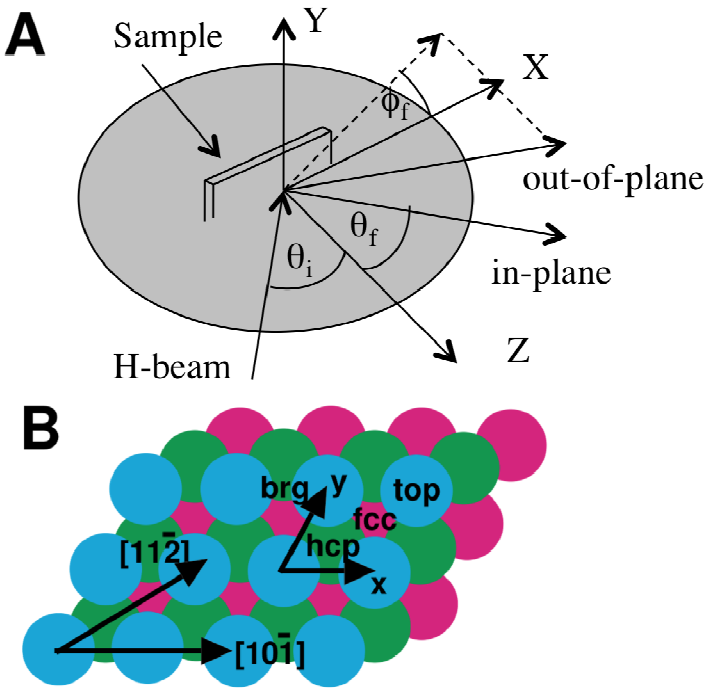

S1. Definition of incidence angle θ_i, and scattering angles θ_f and ϕ_f (A). Plot of the (111) surface of fcc metals like Cu and Au (B). Indicated are the high symmetry sites top, hcp, fcc, and bridge (brg). Also indicated are the crystallographic directions corresponding to the two planes of incidence studied in this work.

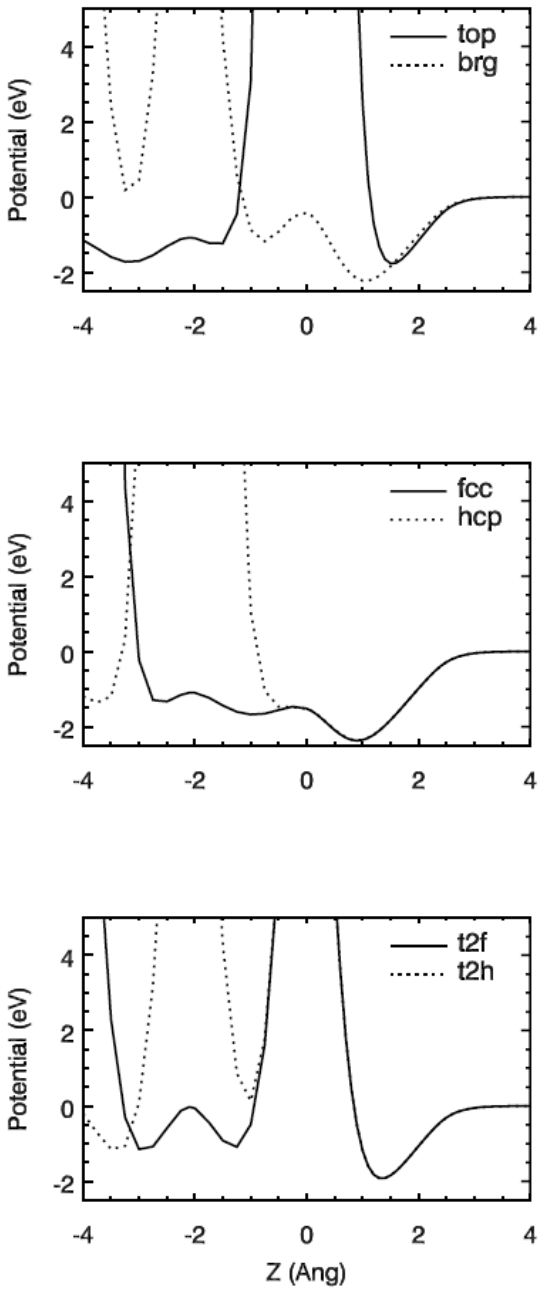

S2. The H-surface interaction potential is shown as a function of the atom-surface distance Z in Å, for H + Cu(111) (see also Fig.S1).

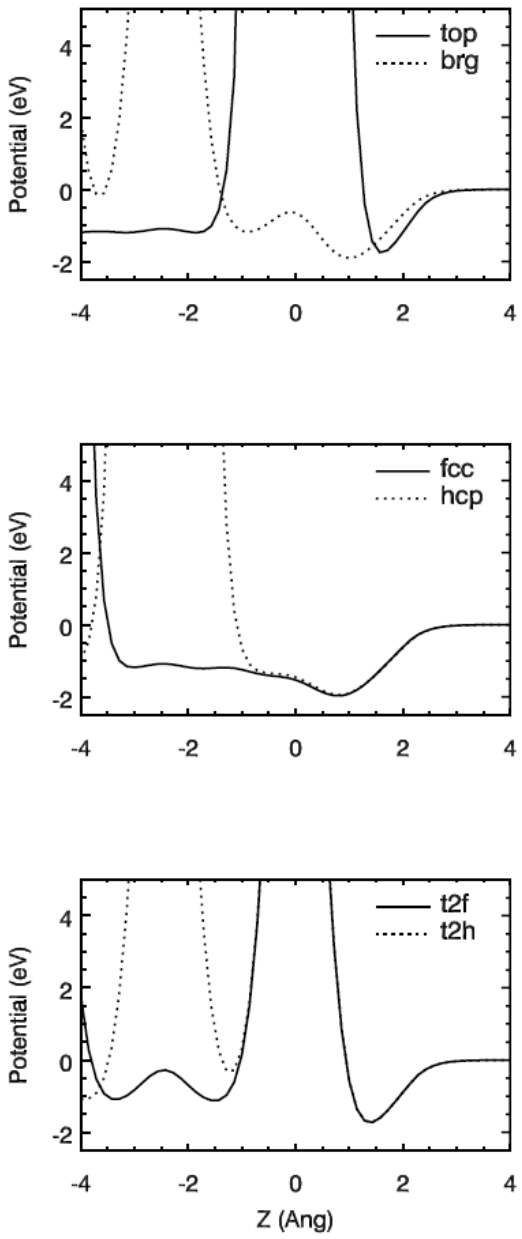

S3. The H-surface interaction potential is shown as a function of the atom-surface distance Z in Å, for H +Au(111) (see also Fig.S1).

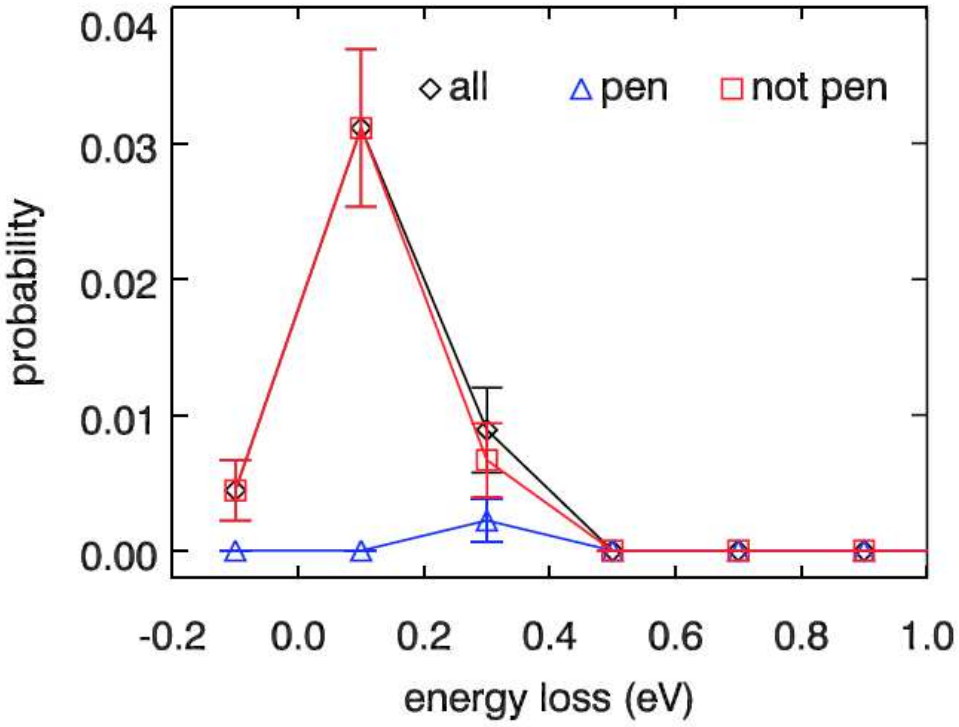

S4. The energy loss distribution for specular scattering is shown of H-atoms that have scattered from the surface ("all"), that have scattered from the surface with penetration of the surface ("pen"), and that have scattered from the surface without penetration of the surface ("not pen"). Results are shown for an incidence energy of 5 eV, for H + Au(111) and θ_i = 60° and ϕ_i=0°.

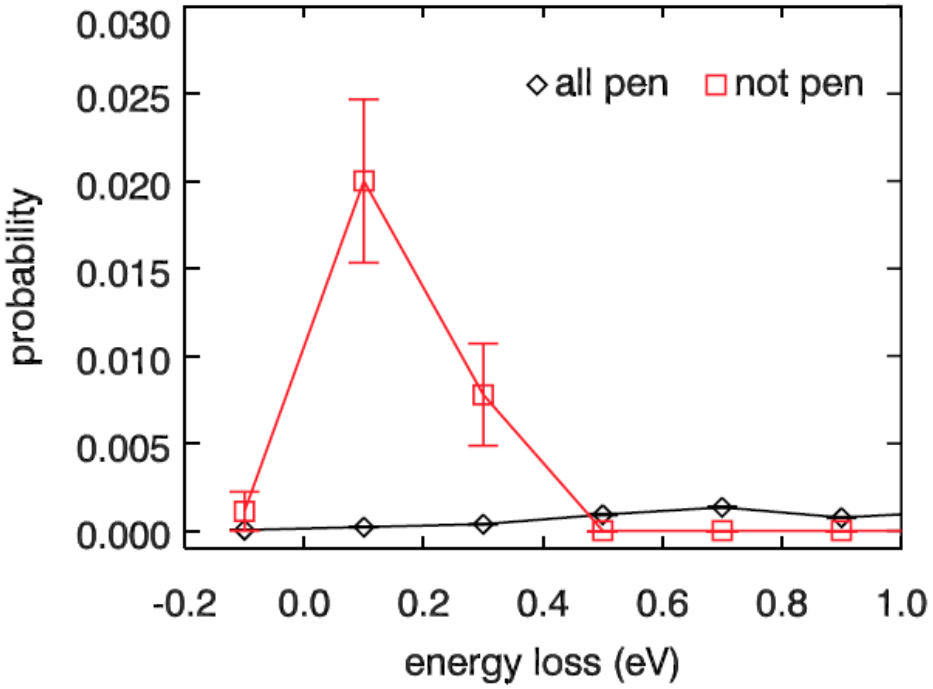

S5. The angularly resolved energy loss distribution is shown for scattering of 5 eV H atoms from Au(111) at $\theta_i = 60°$ and $\phi_i = 0°$ to $\theta_f = 60°$ and $\phi_f = 90°$, at $T_s = 120$ K. In contrast to Fig.4, here a contribution has been taken into account from H-atoms that scatter with penetration at times longer than the timescale of our simulation.

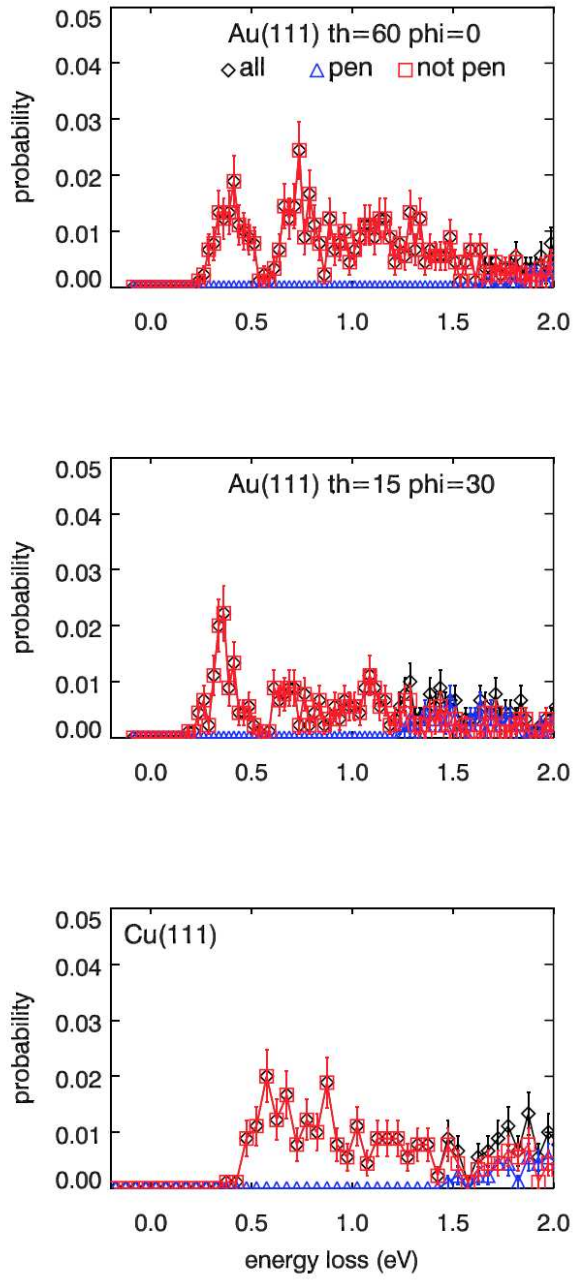

S6. Total energy (adiabatic + non-adiabatic) loss distributions for 5 eV H-atoms scattered from Au(111) and Cu(111) at the indicated incidence angles , T_S=120K.

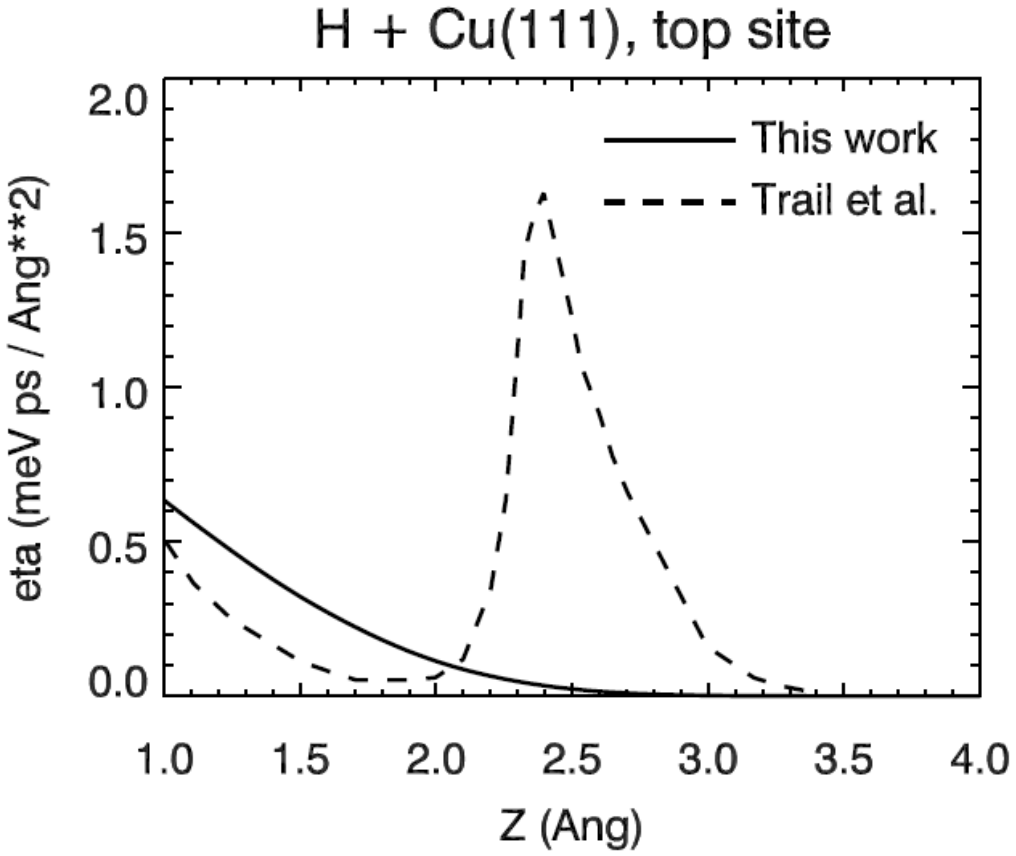

S7. Friction coefficients computed for motion of H along a line that is perpendicular to a Cu(111) surface, and goes through the top site on that surface. Results are shown for the LDFA method [48] used in this work and for the method used by Trail et al. [53].

Table S1. Adiabatic, non-adiabatic, and total energy loss of H-atoms scattering from Au(111) for θ_i =60°, and ϕ_i =0° are presented. Energies are in eV. The aiabatic results were obtained with the AIMD method, and the non-adiabatic results with the AIMDEFp method.

Quantity	Adiabatic	Non-adiabatic	Total
ΔE, all scat	0.21	1.31	1.52
ΔE, scat, no pen	0.14	1.00	1.14
ΔE, scat, pen	0.51	2.58	3.09

References.

(1) Kresse, G.; Hafner, J. Ab-Initio Molecular-Dynamics for Liquid-Metals. *Phys.Rev.B* **1993,** *47*, 558-561.
(2) Kresse, G.; Hafner, J. Ab Initio Molecular-Dynamics Simulation of the Liquid-Metal-Amorphous-Semiconductor Transition in Germanium. *Phys.Rev.B* **1994,** *49*, 14251-14269.
(3) Kresse, G.; Furthmüller, J. Efficiency of Ab-Initio Total Energy Calculations for Metals and Semiconductors Using a Plane-Wave Basis Set. *Comput.Mater.Sci.* **1996,** *6*, 15-50.
(4) Kresse, G.; Furthmüller, J. Efficient Iterative Schemes for Ab Initio Total-Energy Calculations Using a Plane-Wave Basis Set. *Phys.Rev.B* **1996,** *54*, 11169-11186.
(5) Hohenberg, P.; Kohn, W. Inhomogeneous Electron Gas. *Phys.Rev.* **1964,** *136*, B864-B871.
(6) Kohn, W.; Sham, L. J. Self-Consistent Equations Including Exchange and Correlation. *Phys.Rev.* **1965,** *140*, A1133-A1138.
(7) Perdew, J. P.; Burke, K.; Ernzerhof, M. Generalized Gradient Approximation Made Simple. *Phys.Rev.Lett.* **1996,** *77*, 3865-3868.
(8) Hammer, B.; Hansen, L. B.; Nørskov, J. K. Improved Adsorption Energetics within Density-Functional Theory Using Revised Perdew-Burke-Ernzerhof Functionals. *Phys.Rev.B.* **1999,** *59*, 7413-7421.
(9) Díaz, C.; Pijper, E.; Olsen, R. A.; Busnengo, H. F.; Auerbach, D. J.; Kroes, G. J. Chemically Accurate Simulation of a Prototypical Surface Reaction: H_2 Dissociation on Cu(111). *Science* **2009,** *326*, 832-834.
(10) Nattino, F.; Díaz, C.; Jackson, B.; Kroes, G. J. Effect of Surface Motion on the Rotational Quadrupole Alignment Parameter of D_2 Reacting on Cu(111). *Phys.Rev.Lett.* **2012,** *108*, 236104.
(11) Sementa, L.; Wijzenbroek, M.; van Kolck, B. J.; Somers, M. F.; Al-Halabi, A.; Busnengo, H. F.; Olsen, R. A.; Kroes, G. J.; Rutkowski, M.; Thewes, et al. Reactive Scattering of H_2 from Cu(100): Comparison of Dynamics Calculations Based on the Specific Reaction Parameter Approach to Density Functional Theory with Experiment. *J.Chem.Phys.* **2013,** *138*, 044708.
(12) Kresse, G.; Hafner, J. Norm-conserving and Ultrasoft Pseudopotentials for First-row and Transition Elements. *J. Phys.: Condens. Matter* **1994,** *6*, 8245-8257.
(13) Dutta, B. N.; Dayal, B. Lattice Constants and Thermal Expansion of Gold up to 878 °C by X-Ray Method. *Phys. Stat. Sol.* **1963,** *3*, 473-477.
(14) Chae, K. H.; Lu, H. C.; Gustafsson, T. Medium-Energy Ion-Scattering Study of the Temperature Dependence of the Structure of Cu(111). *Phys.Rev.B* **1996,** *54*, 14082-14086.
(15) Zolyomi, V.; Vitos, L.; Kwon, S. K.; Kollar, J. Surface Relaxation and Stress for 5d Transition Metals. *J.Phys.: Conden. Matter* **2009,** *21*, 095007.
(16) Guan, L.; Qiang, X. L.; Janxin Guo, L.; Zhao, Q.; Liu, B. Relaxation and Electronic States of Au(100), (110), and (111) surfaces. *Solid State Comm.* **2009,** *149*, 1561-1564.

(17) Nichols, R. J.; Nouar, T.; Lucas, C. A.; Haiss, W.; Hofer, W. A. Surface Relaxation and Surface Stress of Au(111). *Surf.Sci.* **2002,** *513*, 263-271.
(18) van Hove, M. A.; Tong, S. Y. *Surface Crystallography by LEED: Theory, Computation, and Structural Results*; Springer-Verlag: Berlin; 1979.
(19) Monkhorst, H. J.; Pack, J. D. Special Points for Brillouin-Zone Integrations. *Phys.Rev.B.* **1976,** *13*, 5188-5192.
(20) Pulay, P. Convergence Acceleration of Iterative Sequences. The Case of SCF Iteration. *Chem.Phys.Lett.* **1980,** *73*, 393-398.
(21) Kerker, G. P. Efficient Iteration Scheme for Self-Consistent Pseudopotential Calculations. *Phys.Rev.B* **1981,** *23*, 3082-3084.
(22) VASP, http://cms.mpi.univie.ac.at/vasp/vasp/vasp.html.
(23) Ferrin, P.; Kandoi, S.; Udaykumar Nilekar, A.; Mavrikakis, M. Hydrogen Adsorption, Absorption and Diffusion on and in Transition Metal Surfaces: A DFT Study. *Surf. Sci.* **2012,** *606*, 679-689.
(24) Strömquist, J.; Bengtsson, L.; Persson, M.; Hammer, B. The Dynamics of H Absorption in and Adsorption on Cu(111). *Surf.Sci.* **1998,** *397*, 382-394.
(25) Pan, M.; Flaherty, D. W.; Mullins, C. B. Low-Temperature Hydrogenation of Acetaldehyde to Ethanol on H-Precovered Au(111). *J.Phys.Chem.Lett.* **2011,** *2*, 1363-1367.
(26) Redhead, P. A. Thermal Desorption of Gases. *Vacuum* **1962,** *12*, 203-211.
(27) Gudmundsdóttir, S.; Skúlason, E.; Jónsson, H. Reentrant Mechanism for Associative Desorption: H_2/Pt(110)-(1 x 2). *Phys.Rev.Lett.* **2012,** *108*, 156101.
(28) Bader, R. *Atoms in Molecules: A Quantum Theory*; Oxford University Press: New York; 1990.
(29) Winter, H. Collisions of Atoms and Ions with Surfaces under Grazing Incidence. *Phys.Repts.* **2002,** *367*, 387-582.
(30) Züttel, A. Hydrogen Storage. In *Hydrogen as a Future Energy Carrier*, Züttel, A.; Borgschulte, A.; Schlapbach, L., Eds. Wiley: Weinheim; 2008; pp 165-263.
(31) De Vita, A.; Stich, I.; Gillan, M. J.; Payne, M. C.; Clarke, L. J. Dynamics of Dissociative Chemisorption: Cl_2/Si(111)-(2x1). *Phys.Rev.Lett.* **1993,** *71*, 1276-1279.
(32) Groß, A.; Dianat, A. Hydrogen Dissociation Dynamics on Precovered Pd Surfaces: Langmuir is Still Right. *Phys.Rev.Lett.* **2007,** *98*, 206107.
(33) Groß, A. *Ab Initio* Molecular Dynamics Study of Hot Atom Dynamics after Dissociative Adsorption of H_2 on Pd(100). *Phys.Rev.Lett.* **2009,** *103*, 246101.
(34) Groß, A. Ab Initio Molecular Dynamics Simulations of the Adsorption of H2 on Palladium Surfaces. *Chem.Phys.Chem.* **2010,** *11*, 1374-1381.
(35) Lozano, A.; Gross, A.; Busnengo, H. F. Adsorption Dynamics of H2 on Pd(100) from First Principles. *Phys.Chem.Chem.Phys.* **2009,** *11*, 5814-5822.
(36) Ramos, M.; Martínez, A. E.; Busnengo, H. F. H_2 Dissociation on Individual Pd Atoms Deposited on Cu(111). *Phys.Chem.Chem.Phys.* **2012,** *14*, 303-310.
(37) Groß, A. Ab initio molecular dynamics simulations of the adsorption on complex surfaces. In *Proceedings of the NIC Symposium 2012: 25 Years HLRZ/NIC*, Binder, K.; Münster, G.; Kremer, M., Eds. John van Neuman Institute for Computing: Jülich, 2012; Vol. 45, pp 107-114.

(38) Verlet, L. Computer "Experiments" on Classical Fluids. I. Thermodynamical Properties of Lennard-Jones Molecules. *Phys.Rev.* **1967,** *159*, 98-103.
(39) Verlet, L. Computer "Experiments" on Classical Fluids. II. Thermodynamical Properties of Lennard-Jones Molecules. *Phys.Rev.* **1968,** *165*, 201-214.
(40) Kroeger, F. R.; Swenson, C. A. Absolute Linear Thermal-Expansion Measurements on Copper and Aluminum from 5 to 320 K. *J. Appl. Phys.* **1977,** *48*, 853-864.
(41) Nix, F. C.; MacNair, D. The Thermal Expansion of Pure Metals: Copper, Gold, Aluminum, Nickel, and Iron. *Phys.Rev.* **1941,** *60*, 597-605.
(42) McLean, K. O.; Swenson, C. A.; Case, C. R. Thermal Expansion of Copper, Silver, and Gold Below 30 K. *J. Low Temp. Phys.* **1972,** *7*, 77-98.
(43) Ebert, H. Ausdehnungsmessungen bie tiefen Temperaturen. *Z. Phys. A* **1928,** *47*, 712-722.
(44) Leksina, I. E.; Novikova, S. I. Thermal Expansion of Copper, Silver, and Gold within a Wide Range of Temperatures. *Sov. Phys.-Solid State* **1963,** *5*, 798-801.
(45) Karplus, M.; Porter, R. N.; Sharma, R. D. Exchange Reactions with Activation Energy. I. Simple Barrier Potential for (H,H_2). *J.Chem.Phys.* **1965,** *43*, 3259-3287.
(46) Grimmelmann, E. K.; Tully, J. C.; Helfand, E. Molecular Dynamics of Infrequent Events: Thermal Desorption of Xenon from a Platinum Surface. *J.Chem.Phys.* **1981,** *74*, 5300-5310.
(47) Kroes, G. J. Towards Chemically Accurate Simulation of Molecule-Surface Reactions. *Phys.Chem.Chem.Phys.* **2012,** *14*, 14966-14981.
(48) Juaristi, J. I.; Alducin, M.; Diéz Muiño, R.; Busnengo, H. F.; Salin, A. Role of Electron-Hole Pair Excitations in the Dissociative Adsorption of Diatomic Molecules on Metal Surfaces. *Phys.Rev.Lett.* **2008,** *100*, 116102.
(49) Echenique, P. M.; Nieminen, R. M.; Ritchie, R. H. Density Dunctional Calculation of Stopping Power of an Electron Gas for Slow Ions. *Solid State Commun.* **1981,** *37*, 779-781.
(50) Echenique, P. M.; Nieminen, R. M.; Ashley, J. C.; Ritchie, R. H. Nonlinear Stopping Power of an Electron Gas for Slow Ions. *Phys.Rev.A* **1986,** *33*, 897-904.
(51) Juaristi, J. I.; Arnau, A.; Echenique, P. M.; Auth, C.; Winter, H. Charge State Dependence of the Energy Loss of Slow Ions in Metals. *Phys.Rev.Lett.* **1999,** *82*, 1048-1051.
(52) Winter, H.; Juaristi, J. I.; Nagy, I.; Arnau, A.; Echenique, P. M. Energy Loss of Slow Ions in a Nonuniform Electron Gas. *Phys.Rev.B* **2003,** *67*, 245401.
(53) Trail, J. R.; Bird, D. M.; Persson, M.; Holloway, S. Electron-Hole Pair Creation by Atoms Incident on a Metal Surface. *J.Chem.Phys.* **2003,** *119*, 4539-4549.